ARCTIC COASTAL STORMS, UNIQUE IN CHARACTER AND IMPACT

TOM RAVENS[1], MARTIN HENKE[2], CELSO FERREIRA[2]

1. *College of Engineering, University of Alaska Anchorage, 3211 Providence Drive, Anchorage, AK 99508, USA. tmravens@alaska.edu.*
2. *Sid and Reva Dewberry Department of Civil, Environmental and Infrastructure Engineering, George Mason University, 4400 University Drive, MS-6C1, Fairfax, VA 22030, USA, mhenke@gmu.edu, cferrei3@gmu.edu.*

Abstract: Arctic storm surge events have a distinct character, and their impact on the coast is unique compared to a non-Arctic event. On the one hand, Arctic peak wind speeds rarely reach hurricane strength (74 mph, 64 knots or greater). And pressure drops associated with Arctic storms are small compared to ones in the tropics. More importantly, the impact of an atmospheric storm on the ocean and on the coast is entirely dependent on the season. If a large storm strikes during the winter or when the ocean is ice-covered, the storm will generate negligible waves and surge, and it will not generate erosion or coastal flooding. On the other hand, if a large storm strikes when the ocean is partially ice-covered (e.g., 50% covered), surge may be enhanced relative to an ice-free ocean, potentially leading to greater coastal flooding.

Introduction

With a partially ice-covered ocean, wave action would be significantly reduced and so would wave setup, wave runup, and coastal erosion. With essentially no ice (or with the ice pack far offshore), then the role of sea ice becomes minimal. However, the impact of the storm on geomorphology will be very different in the Arctic compared to its impact in a non-Arctic setting because of the presence of coastal permafrost. Coastal processes (including erosion) include important thermal components as well as mechanical ones. Sediment along the coast needs to be thawed before it is available for transport by mechanical forces. If a given storm strikes early in the open water season, the potential geomorphic change will be significantly reduced because much of the coast will be frozen. As a final note, it is important to note that climate warming is having long-term impacts on the thermal environment of the Arctic coast and its permafrost. Thawing of the coastal permafrost is expected to lead to subsidence of the coast by as much as 1 ft by 2100. Hence, a given Arctic storm will over time cause more flooding due to this Arctic enhancement in relative sea level rise. In this paper, we introduce the 5 interdependent coastal hazards caused by Arctic storms and discuss how the hazards are enhanced by climate change. Second, we discuss how storm surge and storm waves are affected by the presence of sea ice, we show how climate change

has made coastal waves significantly larger. Third, we introduce the two main Arctic coastal erosion mechanisms active on the Alaska Beaufort coast and show how erosion is enhanced by climate change.

1. Interdependent coastal hazards caused by Arctic storms and climate change

Arctic coastal storms generate 5 interdependent coastal hazards including waves, coastal erosion, permafrost thaw and subsidence, storm surge and flooding, and salinity intrusion (Figure 1, blue boxes). Permafrost thaw and the resulting subsidence are unique to the Arctic, and we will focus on this hazard here. Coastal sediments are typically locked in place by permafrost and thawing of the permafrost is a prerequisite for later removal by mechanical processes. Thus, coastal permafrost thaw enhances coastal erosion. Coastal permafrost thaw and the subsequent subsidence also effectively enhances coastal water levels and coastal flooding. Further, flooding in the Arctic enhances permafrost thaw and subsidence in a positive feedback loop.

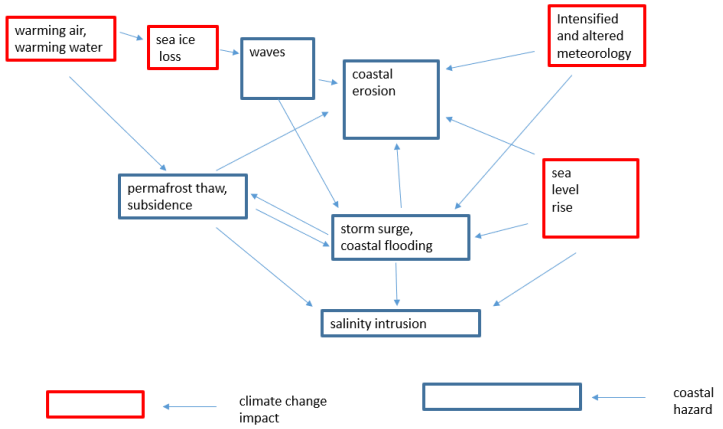

Figure 1. Flow chart depicting the interdependence of the 5 Arctic coastal hazards and the impact of climate change on those hazards.

Each of the hazards are enhanced by climate change (Figure 2, red boxes). For example, the warming air and water is increasing the permafrost thaw rate contributing to accelerating coastal erosion. Warming air and water are also causing sea ice loss which increases fetch leading to larger waves (Overeem et al., 2011) and enhanced erosion (Kobayashi et al., 1999).

2. The effect of reduced sea ice on storm waves

Kasper et al. (2023) recently developed a high-resolution (nested) hydrodynamic

and wave model for Foggy Island Bay on the north coast of Alaska, for the period 1979-2019 (Figure 2). The model documented the dramatic increase in coastal wave height on the Alaska Beaufort coast due to sea ice reduction between 1979 and 2019. Boundary data for the nested wave model came from the 30-km resolution ERA5 Reanalysis product, developed by the European Centre for Medium-Range Weather Forecasts (ECMWF), (https://cds.climate.copernicus.eu/cdsapp#!/home).

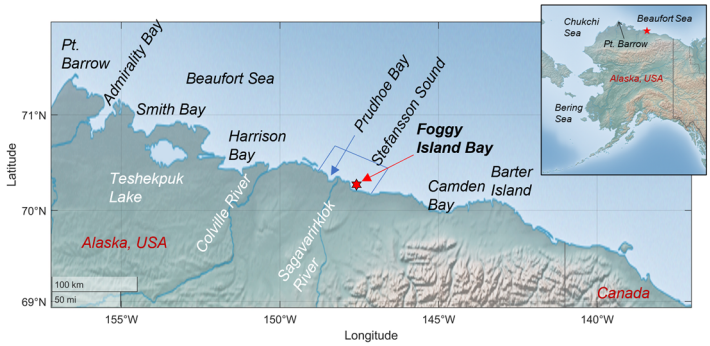

Figure 2. Map of the Alaska Beaufort Sea coast, including the Foggy Island Bay study site. Reprinted from Kasper et al., 2023.

An unstructured mesh hydrodynamic model (Delft3D4-FM) with a coastal resolution on the order of 2 km encompassing the entire state of Alaska was used to estimate storm surge and tidal water level variations. The Delft3D FM hydrodynamic model encompassed the entire State of Alaska and covered an area of 7,506 km by 3,586 km, including 29,656 nodes. Water level at the boundary was based on FES2014 tidal constituents (Lyard et al., 2021). Atmospheric forcing was based on ERA5 data. The effect of sea ice concentration on wind drag was based on the work of Garratt (1977), Lüpkes et al. (2012) and Joyce et al., (2019). Figure 3 documents the use of measured wave data for model calibration and assessment.

Figure 4 provides the daily median wave height and sea ice concentration across Foggy Island Bay for 1979-2019. The increase in wave height, the reduction in sea ice, and the lengthening of the open water period between 1979 and 2019 are readily apparent. Nederhoff et al. 2022, reporting from the same study, found a small increase in wave period of up to 0.03 s/yr in the deeper Bay between 1979–2019. While surge events were observed to increase with the increase in open water period at a rate of 0.13 events per day of increase in the open water season, Kasper et al. (2023) reported a small but statistically significant negative trend (-0.2 cm/year) of the 3-year moving mean annual maximum storm surge.

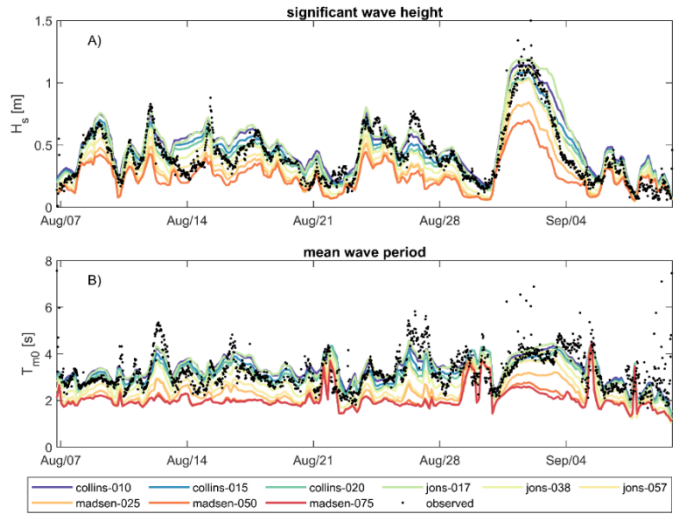

Figure 3. Calibration and sensitivity testing of bottom friction settings for the nested wave model. The location of model assessment was "Spotter 0156" (70.31882, -147.76044) in a mean water depth of 3.2 m. Reprinted from Nederhoff et al., 2022.

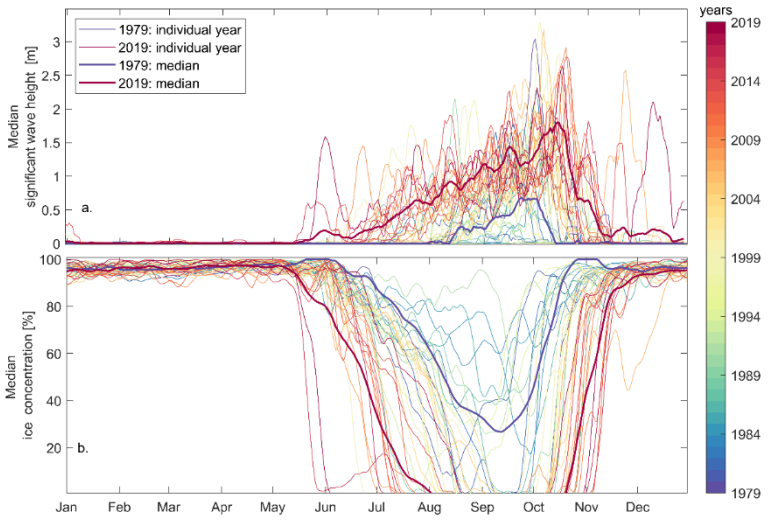

Figure 4. Median wave height (a) and sea ice (b) concentration in Foggy Island Bay between 1979-2019. Reprinted from Nederhoff et al., 2022.

3. Arctic storm-induced coastal geomorphic change

In order to explore the impact of Arctic storms on coastal change, we will consider

two different perspectives. In the first perspective, we will consider a generic coastal configuration consisting of a frozen coastal bluff (e.g., Kobayashi et al., 1999). In the second perspective, we will consider the actual coastal erosion mechanisms that are predominant on the Alaska Beaufort Sea coast.

3a. The impact of Arctic storms considering a generic coastal configuration

In their pioneering Arctic coastal erosion work, Kobayashi et al. (1999) considered an idealized beach and bluff (cliff) profile that was largely frozen (Figure 5), and they determined the retreat rate of the bluff based on the heat transfer rate to the bluff and based on the heat of fusion of bluff materials.

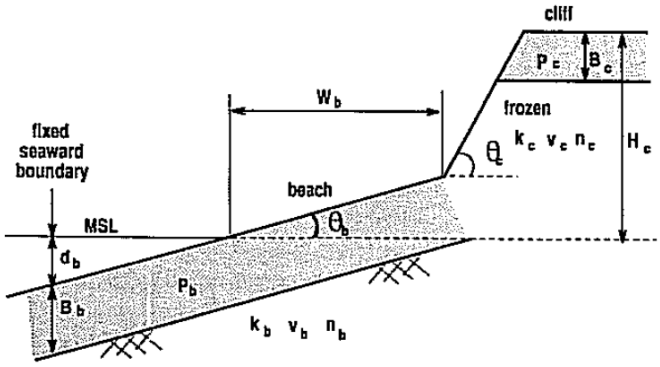

Figure 5. Idealized beach and bluff (cliff) considered by Kobayashi et al. 1999 (Reprinted from Kobayashi et al., 1999).

Building on this work, Ravens et al. (2017) developed an Arctic-capable coastal geomorphic change model, assuming a coastal configuration similar to that assumed by Kobayashi (1999, Figure 5). The model (referred to as "Arctic Xbeach") was a coupling of an existing open source non-Arctic coastal geomorphic change model (Xbeach, Roelvink et al., 2010) with a thermal model. The thermal model determined the temperature and phase of the soils and sediments, and Xbeach determined the potential geomorphic change considering the offshore wave and water level climate. However, that potential was only actualized if the soil and sediment was determined to be unfrozen by the thermal model.

One relevant insight from the development and application of Arctic Xbeach was that the geomorphic change determined by a given storm is dependent on the timing of the storm. If a storm strikes early in the open water period when the soil and sediment is still frozen, the geomorphic change caused by the storm will be

small compared to the change caused if the storm struck later in the season after the surface soil and sediment had thawed. To illustrate this point, a 2-day synthetic storm with a 2-m wave height and a 0.5 m surge height (Figure 6a) was considered. In the first simulation, we assumed air, water, and initial soil/sediment temperature was 5C, 2C, and -2C, respectively, and we computed the change in the bluff/beach profile (Figure 6b). Figure 6b also includes the post-storm profile if we that there was no permafrost in the soil/sediment. The results show that if the soil and sediment are initially frozen (and with a temperature of -2C), there is relatively little geomorphic change. On the other hand, if we model this coastal configuration ignoring the presence of permafrost, we see that there would be a significant amount of unrealistic geomorphic change. In a second simulation, we assumed the same storm and compared the calculated geomorphic change

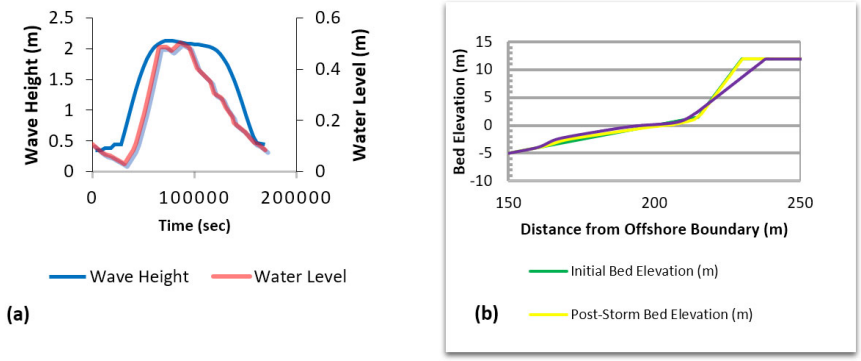

Figure 6. (a) Assumed offshore wave height and water level and (b) initial and post-storm beach and bluff profile. Reprinted from Ravens et al., 2017.

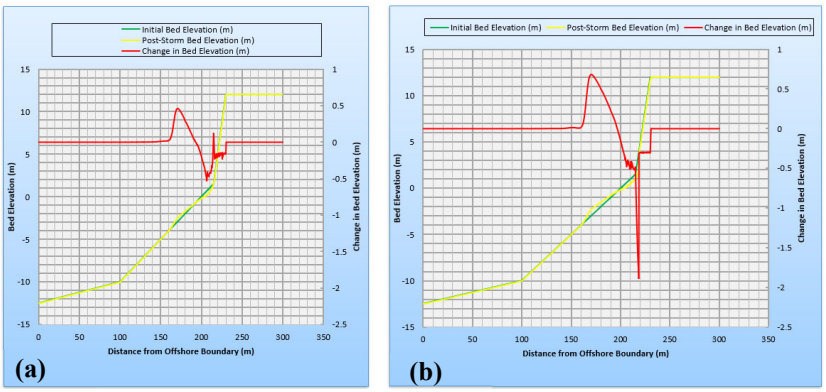

Figure 7. Initial bed elevation, post-storm elevation, and change in bed elevation assuming (a) initially frozen soil and sediment and (b) an initial thaw depth of 30 cm in soil and sediment. Reprinted from Ravens et al., 2017.

assuming (a) permafrost in soil and sediment initially at a temperature of -2C (as in Figure 6), and (b) the soil and sediment had thawed to a depth of 30 cm at the start of the storm (Figure 7). The Figure shows that the storm-induced geomorphic change is significantly greater if the soil/sediment had thawed to a depth of 30 cm prior to the storm. Thus, in an Arctic setting, the amount of geomorphic change due to a given storm is dependent on the timing of the storm.

3b. The impact of Arctic storms considering the predominant coastal erosion mechanisms

The two main erosion mechanisms on the Alaska Beaufort Sea coast include niche erosion/block collapse (or thermal abrasion) and bluff face thaw/slump (or thermal denudation). The impact of an Arctic storm on the coast depends on the particular coastal location and the erosion mechanism that is active there. Niche erosion/block collapse (Kobayashi, 1985; Ravens et al., 2012; Barnhardt et al., 2014) causes the highest annual rates of coastal erosion and is predominant at coastal bluffs in locations like Drew Point, Cape Halkett, and Elson Lagoon which lack coarse sediments (sand and gravel) and which lack a significant beach (Figures 8-9). As a consequence of the low elevation beach, even a relatively small storm surge leads to coastal bluff and niche erosion. A conceptual model of niche erosion/block collapse is presented in Figure 10. Typically, there is a small beach before the coastal bluff. During a storm surge event, water levels rise allowing the ocean water to directly contact the bluff. The waves and currents thermally and mechanically cut a niche into the bluff. The niche grows until the over burden exceeds the strength of the bluff leading to block collapse. Failure of the coastal bluffs often occurs along ice wedges (evident in Figure 9b) which are

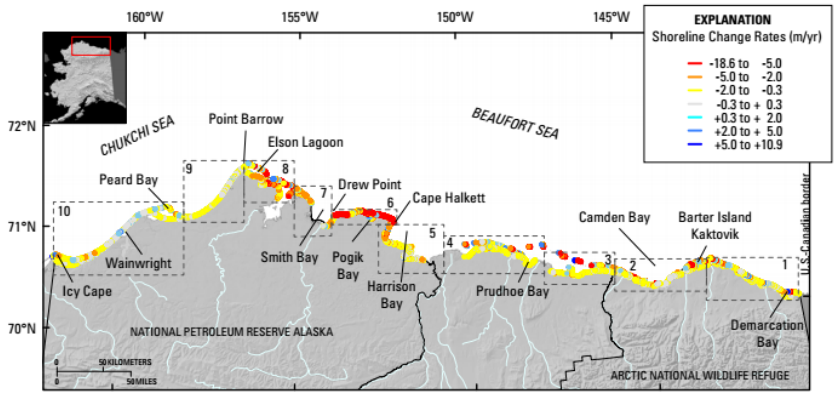

Figure 8. Map of the north coast of Alaska showing color-coded shoreline change rates for the period circa-1940's (1947 and 1949) to circa-2000's (1997–2012). Reprinted from Gibbs and Richmond, 2015.

linear ice features in the near-surface geology with, typically, a wedge-shaped cross-section (Harry and Gozdzik, 1988). Once a block has collapsed, waves and currents thermally and mechanically erode the fallen block. The solid materials in the block are mainly fine sediments that are readily dispersed by the waves and currents.

Figure 9. Photos of (a) an erosional niche from Elson Lagoon Alaska and (b) a fallen block by Drew Point, Alaska (image courtesy of Christopher Arp of the Alaska Science Center, U.S. Geological Survey). Reprinted from Ravens and Peterson, 2021.

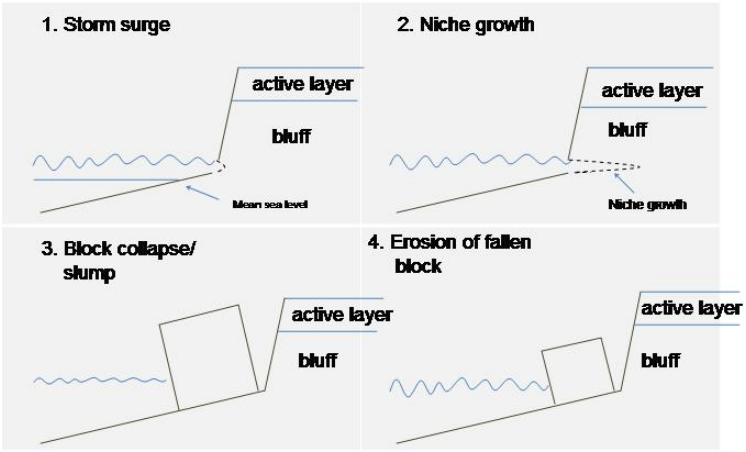

Figure 10. Conceptual model of the niche erosion/block collapse erosion mechanism. Reprinted from Ravens et al., 2012.

The niche erosion/block collapse mechanism is dominant where the coastal bluffs are ice rich (~70% by volume, Ping et al., 2011) and lacking coarse sediments. Under such a situation, the beach before the bluff has a low elevation and contact between the Sea and bluff is frequent. In other settings, the coastal bluffs have significant quantities of coarse sediments (sand and gravel, Figure 11). As a consequence, the beach before the bluff has a relatively high elevation (1 to 2 m above mean sea level) and contact between the Sea and the bluff toe – and niche erosion - is infrequent (Ravens et al., 2011). Coastal erosion in this setting is

Figure 11. Photo showing material that has slumped onto the beach face following bluff face thaw at Barter Island, north coast Alaska. Reprinted from Ravens and Peterson, 2021.

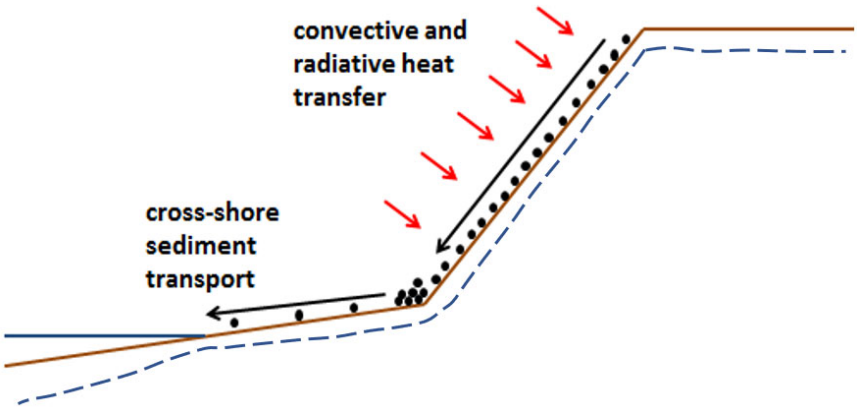

Figure 12. Sketch depicting the bluff face thaw/slump mechanism including the thawing and slumping of the bluff face (step 1) and the offshore transport of sediment deposited on the beach (step 2). The dashed blue line indicates the thaw line.

driven by the thawing and slumping of the bluff face, the deposition of the material on the beach face, and the transport of material offshore due to storm-induced cross-shore transport – shown conceptually in Figure 12. Here, we refer to this erosion mechanism as bluff face/thaw slump, but it is also referred to as translational-shear ice-thaw (Gibbs et al., 2013) and thermal denudation.

Ravens and Peterson (2021) identified a single parameter – coarse sediment aerial density – that controls which of these two erosion mechanisms are dominant in Arctic Alaska. The coarse sediment aerial density is the dry mass of coarse sediment (sand and gravel) contained in a column of bluff sediment/soil per unit horizontal area (g cm^{-2}). Ravens and Peterson (2021) examined 22 coastal sites in Arctic Alaska. They inferred coastal erosion mechanism based on aerial photos (Gibbs and Richmond, 2009) and gathered data on sediment aerial density based on available soil core data (Ping et al., 2011). The sites were distributed across the north coast of Alaska between Barrow and the Canadian border (Figure 13). The erosion mechanism was found to be tied to the coarse sediment aerial density. With sediment aerial density greater than 120 g cm^{-2} the dominant erosion mechanism was bluff face thaw/slumping. With sediment aerial density less than 80 g cm^{-2}, the dominant erosion mechanism was niche erosion/block collapse (Figure 14).

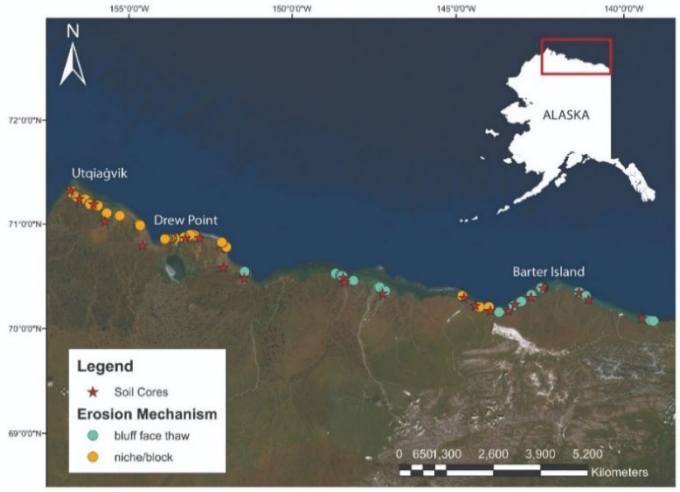

Figure 13. Map of the north coast of Alaska showing the locations of the coastal sites studied as well as the erosion mechanism attributed to those sites. Base map imagery courtesy of Esri. Reprinted from Ravens and Peterson, 2021.

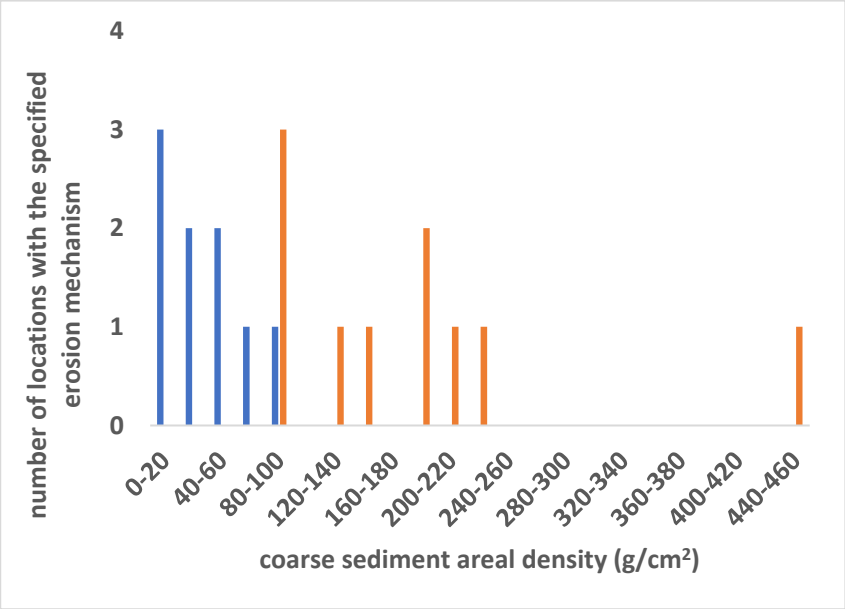

Figure 14. A histogram showing the frequency of occurrence of the niche erosion/block collapse erosion mechanism and bluff face thaw/slump mechanism as a function of coarse sediment areal density. Reprinted from Ravens and Peterson, 2021.

Arctic coastal erosion modeling efforts – Niche erosion/block collapse

One of the most dramatic forms of coastal erosion and the "poster child" of Arctic coastal erosion is the niche erosion/block collapse erosion mechanism (Figures 9-10). Niche erosion/block collapse is responsible for some of the highest rates of coastal erosion in the Arctic with rates as a high as 15 m/yr in Arctic Alaska (Barnhart et al., 2014b).

The critical, rate-determining step is the niche erosion process (Ravens et al., 2012). Kobayashi (1985) developed a niche erosion model founded on three partial differential equations based on mass balances of salt and suspended sediment, and a heat balance of a sediment/water mixture. The analysis assumed a storm surge event that instantaneously raised water levels to a depth of h at the coast (Figure 15). It also assumed surf zone conditions and vertically well-mixed water properties near the coast.

Assuming that the surf zone diffusivities for mass and heat transfer can be estimated based on a surf zone eddy diffusivity and assuming the physical and

thermal properties of seawater and frozen sediment are constant, the differential equations are amenable to an analytical solution:

$$x_m = 2\,\varepsilon_m\sqrt{\varepsilon\,t} \tag{1}$$

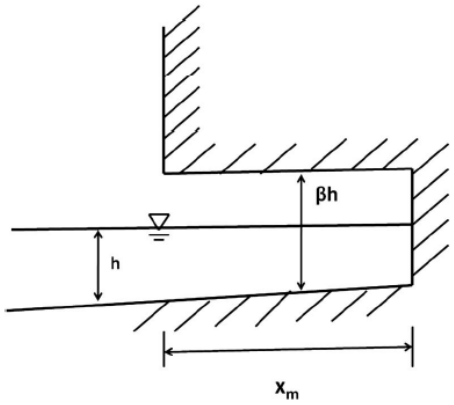

Figure 15. Schematic of conditions assumed in the Kobayashi niche erosion model (Reprinted from Ravens et al., 2012).

where x_m is the position of the melting front, assumed equal to zero at start of niche erosion,
ε_m is a temperature dependent parameter which is approximately 0.0094 T_d, assuming negligible suspended sediment before the storm and 30 ppt salinity,
T_d = T_w-T_m is the difference between the temperature of the nearshore water (T_w) and the melting point of the interstitial water holding the bluff material together (0C).
ε is the momentum diffusivity of the longshore current due to breaking waves assumed to be $Ah(gh)^{1/2}$ (Longuet Higgins, 1970),
A is an empirical constant assumed to be 0.4, and
h is the water depth in the niche and adjacent nearshore waters which is assumed to be constant.

Examination of Eq. (1) indicates that the rate of niche erosion (dx_m/dt) is proportional to the temperature difference between the nearshore water and the melting point of the ice in the bluff, and proportional to water depth to the ¾ power. Given that the ratio of the wave height to water depth in the surf zone is constant, Eq. (1) also indicates that the niche erosion rate is proposition to wave height to the ¾ power. The temperature difference can be considered the thermal driver of niche erosion; wave height (to the ¾ power) can be considered the

mechanical driver. During a large Arctic storm with winds from the west or northwest, both a high surge and large waves can be expected (if sea ice is absent) and the rate of niche erosion can be expected to be quite high, especially if the storm strikes late in the open water period when water temperatures are elevated.

Ravens et al. (2012) built an integrated system of models based on the conceptual model above, producing a predictive, process-based coastal erosion (shoreline change) model for Drew Point on the north coast of Alaska (Figures 8-9). The system of models included a storm surge model, a niche erosion model, a wave model, and a block erosion model. The storm surge model was developed based on the cross-shore equation of motion (Dean and Dalrymple, 2004) assuming a long and straight coastline (Eq. (2)):

$$g(h_m + \eta)\frac{\partial \eta}{\partial x} = (h_m + \eta)fV + \frac{\tau_{sx}}{\rho} \quad (2)$$

where g is the gravitational acceleration,
h_m is the mean water depth,
x is onshore directed position coordinate,
y is the coordinate indicating alongshore position,
f is the Coriolis frequency (= $2\Omega\sin\varphi$),
Ω is the angular frequency of the earth (7.272×10^{-5} rad/s),
φ is the latitude of the study site,
ρ is sea water density (~1020 kg m^{-3}),
V is the (depth-averaged) alongshore water velocity (defined below), and
τ_{sx} is the wind stress on the water surface in the onshore direction.

A niche erosion model was developed based on the work of Kobayashi (1985) described above. Block collapse was not explicitly modeled. Instead, block collapse was assumed to occur when the position of the melting front (x_m) reached a preset distance (nominally 10 m based on observations of the dimensions of fallen blocks, but 5 m was also considered). Finally, an empirical block erosion model was developed assuming that the erosion amount in a 12 hour period (ER, kg/m alongshore) was dependent on temperature difference (T_d) between the nearshore water and the melting point of soil interstitial ice and on the wave height (H, at 3 m depth) according to:

$$ER = aH^n T_d \quad (3)$$

where a and n are empirical constants.

Ravens et al. (2012) modeled shoreline change over relatively long time periods (e.g., 1979-2002). The multi-year time period was divided into 12 (or 6) hour time blocks and the relevant environmental data (nearshore water surface elevation, nearshore water temperature, and nearshore wave height) was computed for each

time block. Nearshore water surface elevation was computed with the storm surge model using measured meteorological data from Utqiagvik (formerly Barrow) Alaska for model forcing. Nearshore water temperature was calculated with an ocean/sea ice model (Zhang et al., 2010), and nearshore wave height (computed at a location offshore of the study site in 3 m of water) was computed with a quasi-steady SWAN wave model. For simplicity, an average nearshore water temperature was determined for each month of the open water period (July, August, September, and October) for the time period of interest. Similarly, an average ice edge position was computed for each of the four months for the time period of interest in order to define the open water extent and compute the nearshore wave condition.

Ravens et al. (2012) used the 1979-2002 time period for model calibration determining the optimal empirical constants (a and n) to be 800 kg $(m°C)^{-1}$ and 1.47, respectively. A third model parameter, the elevation of the beach before the bluff, was set to 0.58 m to optimize the calculations. A second time period 2002-2007 was used for model validation. Table 1 (below) from Ravens et al. (2012) depicts the agreement between model and measurements for the calibration and validation time periods. The relatively simple model provided accurate calculations with predicted shoreline change in agreement with measurements within measurement uncertainty. A sensitivity analysis indicated that the observed increase in erosion rate in the later period (2002-2007) was largely due to warmer nearshore waters with the changed meteorological conditions actually contributing to a reduction in shoreline change rate. The shoreline change rate was found to be sensitive to the beach elevation used, with a lower beach elevation translating to more frequent contact between the relatively warm sea-water and the coastal bluff – translating to increased erosion rate. Surprisingly, the increase in open water extent in the later period was found to be a relatively small contributor to the erosion rate increase. Reducing the critical depth of niche erosion before block collapse (from 10 m to 5 m) was calculated to reduce erosion rates by about 20%.

Table 1. Measured and modeled shoreline change rates at Drew Points for two time periods.

Time period	Measured erosion rate (m/yr)	Modeled erosion rate (m/yr)
August 1979–July 2002	8.0 ± 0.9	8.0 ± 0.8
August 2002–July 2007	14.1 ± 1.7	14.9 ± 1.4

Above, we discussed how climate change was reducing sea ice and increasing wave height, wave period and open water period. The increase in open water period was tied to an increase in storm surge events that are at the heart of this erosion mechanism. These considerations indicate that Arctic storms will erode the coast at locations where niche erosion/block erosion is dominant even more

rapidly as climate change continues. Indeed, the increase in erosion rate in the latter period is a direct effect of climate change.

Arctic coastal erosion modeling efforts – Bluff face thaw/slump

The bluff face thaw/slump erosion mechanism described above is responsible for erosion at the majority of the Alaska Beaufort Sea shoreline though the erosion rates with this mechanism are generally smaller than erosion under niche erosion/block collapse mechanism. Below, a two-step bluff face thaw/slump erosion model for the Foggy Island Bay (the focus of the storm simulations described in section 2 of this paper) is described. The specific location of the model was a single USGS transect (#2112), with offshore and onshore end points of 481849.7 E, 7788118.9 N and 481607.2 E, 7787625.2 N, UTM Zone 6, respectively (Figure 16). Analysis of shoreline position data by USGS transect #2112 from 2007 to 2018 (Figure 17) indicates that the average bluff and shoreline retreat rate is about 1.5 m/year.

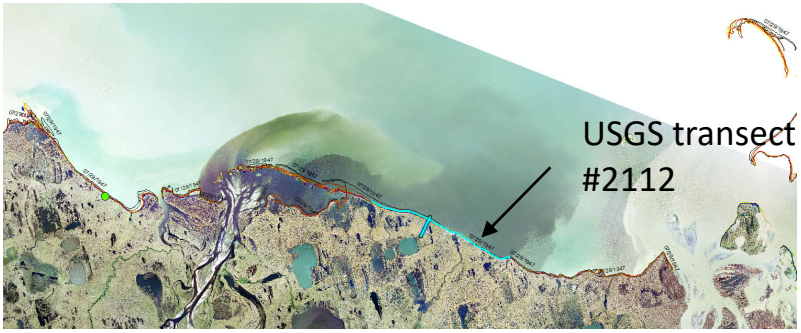

Figure 16. Aerial photo of Foggy Island Bay coastal zone and the location of USGS transect #2112. Reprinted from Kasper et al., 2023.

Figure 18 provides an aerial photo of the bluff and beach face proximal to USGS transect #2112, and it enables insight into the erosion mechanism. A close look at Figure 18 shows tundra vegetation sliding down the bluff face, indicating thawing of the bluff face and slumping of bluff face materials to the beach face. Coastal erosion at this location (and at most locations on the Alaska Beaufort coast) proceeds via a two-step process (Ravens and Peterson, 2021). In the first step, which occurs mainly during inter-storm periods, the bluff face thaws and thawed material slumps and deposits on the beach face (Figure 19). Solar radiation, longwave radiation (emitted from earth surface and downward from atmosphere), sensible heat, and latent heat fluxes combine to thaw the bluff face. In the second step, which occurs during storm periods, storm surges and waves transport slumped materials offshore.

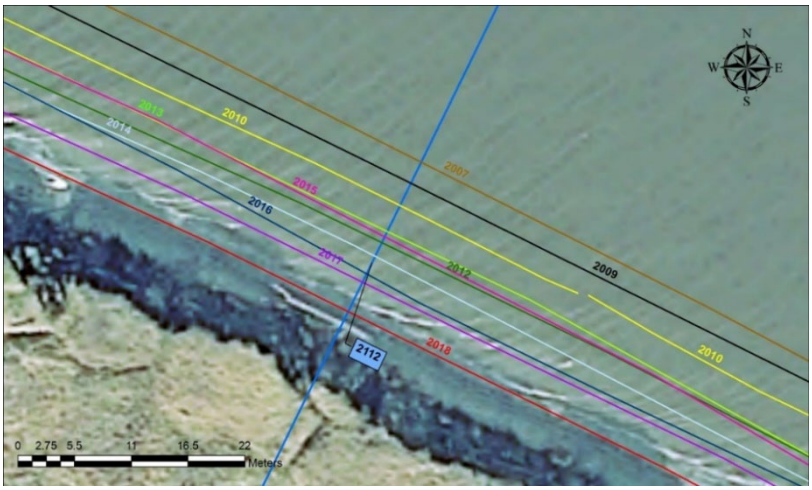

Figure 17. Depiction of Foggy Island Bay shorelines between 2007 and 2018, proximal to USGS transect #2112. Reprinted from Kasper et al., 2023.

Figure 18. Clip of a USGS aerial photo image of shoreline by USGS transect #2112. Reprinted from Kasper et al., 2023.

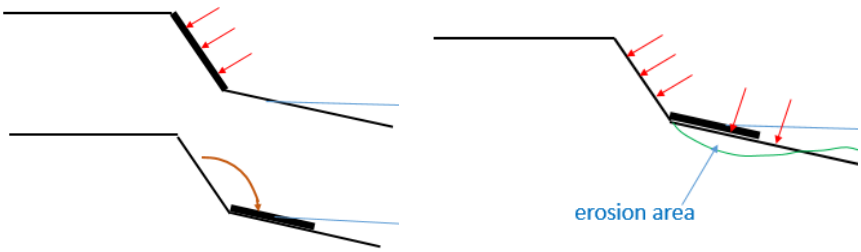

Figure 19. Schematic of the two-step erosion mechanism featuring (a) bluff face thaw/slump, followed by (b) offshore transport during storm surge events. Reprinted from Kasper et al., 2023.

To represent the first step of the two-step sequence, a 1D thermal model – oriented perpendicular to the bluff face – was developed to predict ground temperature and

phase, and it has been validated using available ground temperature data. For the second step, we have coupled the heat transfer model with an open source coastal geomorphic change model, Xbeach. The Xbeach user provides the bluff and beach topography and bathymetry, sediment grain size, and the offshore wave and water level boundary condition – and Xbeach provides the change in the beach profile. Recall, with Arctic Xbeach, material is allowed to move only if it has been thawed. However, in this particular application, we expected limited benefits from using Arctic Xbeach and ran the simpler Xbeach model to represent storm-driven offshore transport in step 2.

The concept of the inter-storm/storm sequence is illustrated in Figure 20. The figure depicts nearshore water level (including tides and storm surge at 5 m depth offshore) as well as wave height for the month of June and July, 2017. The data shows some storm surge events in the month of June. However, due to the presence of sea ice, there is little wave action until the month of July 2017. For effectual offshore transport of sediments, it is necessary to have both significant surge (η > 0.4 m) and significant wave height (H > 0.4 m). Since, coincident significant surge and wave height do not occur until July 20, the period between June 1 and July 19 can be considered an inter-storm period.

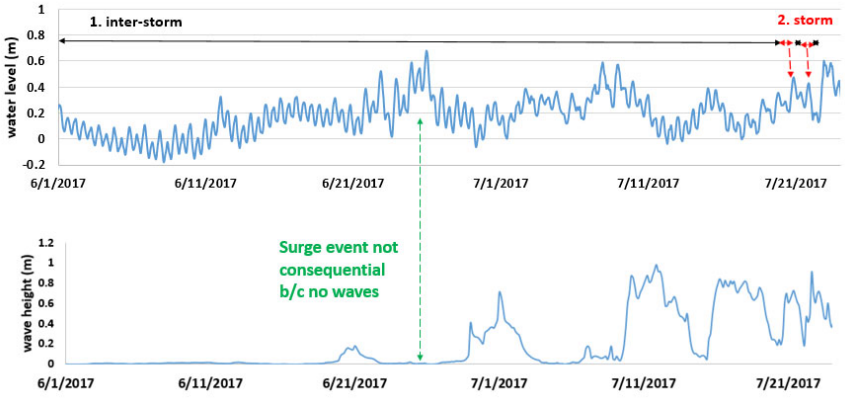

Figure 20. Plots of water level and wave height in June and July 2017. Black and red double arrows at the top of the figure depict the inter-storm and storm periods. Reprinted from Kasper et al., 2023.

The 1D numerical thermal model to determine the bluff face thaw during the inter-storm periods was developed based on the 1D time-dependent heat balance equation in terms of enthalpy, H (Hu and Argyropoulos, 1996):

$$\rho \frac{\partial H}{\partial t} = \nabla \cdot (K \nabla T) \tag{4}$$

Where $H = c_s\ T \qquad for\ T < T_m$
$H = c_l\ T + (c_s - c_l)\ T_m + L \qquad for\ T \geq T_m$
$c_s =$ specific heat of the solid phase
$c_l =$ specific heat of the liquid phase
$T_m =$ temperature of melting
$L =$ latent heat.

Validation of the two-step erosion model

The 1D numerical model was validated by simulating the "Stephan problem" and comparing the numerical solution to the published analytical solution (Hu and Argyropoulos, 1996). In the Stephan problem considered here, there is a 1D bar with the properties of water, extending from y = 0 to y = ∞. The initial temperature is -5C (Figure 21). At t = 0, the surface (y = 0) is set to 2 C, and heat flows from the surface into the bar (in the positive y direction). The numeral solution and the analytic solution (Hu and Argyropoulos, 1996) at 10^5 seconds are shown to be in reasonable agreement (Figure 21).

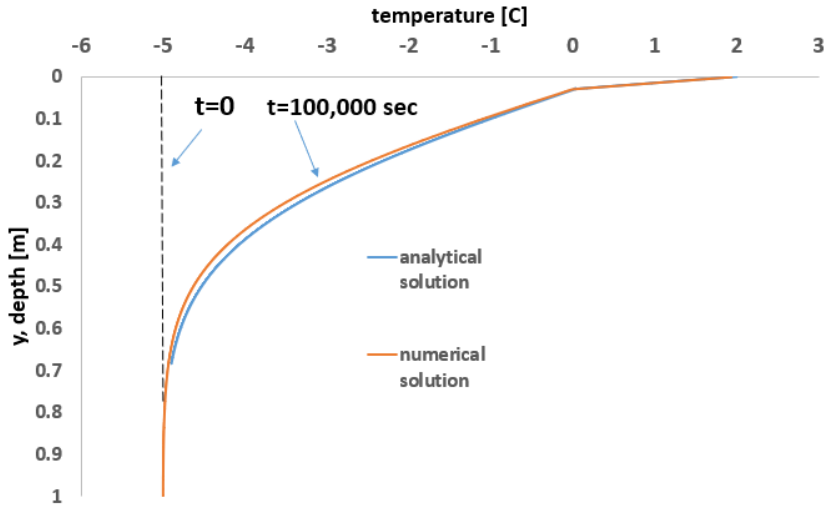

Figure 21. Depiction of the initial temperature and the analytical and numerical solution to the Stephan problem at 10^5 seconds. Reprinted from Kasper et al., 2023.

The 1D thermal model was also validated using ground temperature data from West Dock, which is proximal to Foggy Island Bay, Alaska. In this situation, we defined an initial, June 1, 2017 temperature distribution from the surface to a depth of 10 m, based on West Dock ground temperature data (https://permafrost.gi.alaska.edu). The model was "forced" using measured surface temperature data. Comparison of

the modelled and measured ground temperature data on Aug. 24, 2017, with the thermal properties shown in Figure 22, demonstrated a second validation of the 1D thermal model.

In addition, the 1D thermal model was validated for the case where a flux-type boundary condition was used at the tundra surface. The net heat flux was the sum of the solar (short wave) radiation, the longwave radiation emitted from the earth's surface, the downward longwave radiation from the atmosphere, the latent heat flux, and the sensible heat flux (Figure 23). Note, over the time period used in the figure (between July 14 and Aug. 13, 2017), solar shortwave radiation (in red) diminishes significantly and so does the net heat flux (in blue). As shown in Figure 24, the modelled and measured Aug. 24 2017 ground temperature were in reasonable agreement when the flux-type boundary condition was used. In addition, the modelled and measure thaw depth were also in agreement when the flux-type boundary was employed (Figure 25).

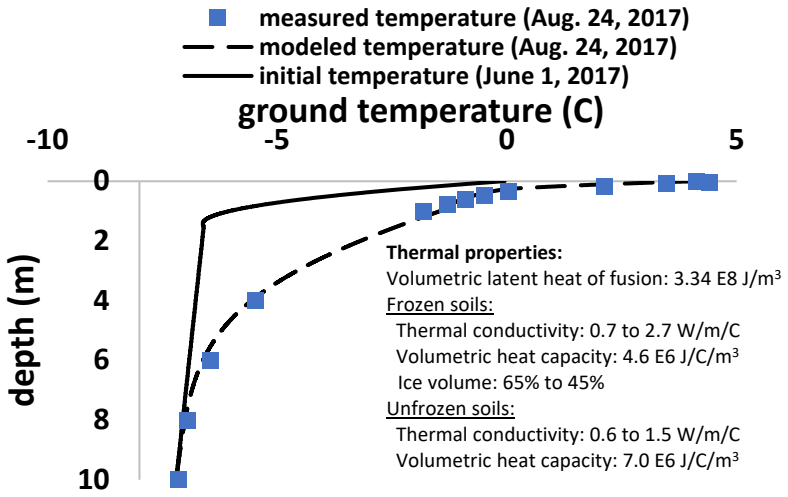

Figure 22. Depiction of the initial temperature distribution on June 21, 2017 along with the modelled and measured temperature distribution on Aug. 24, 2017. Reprinted from Kasper et al., 2023.

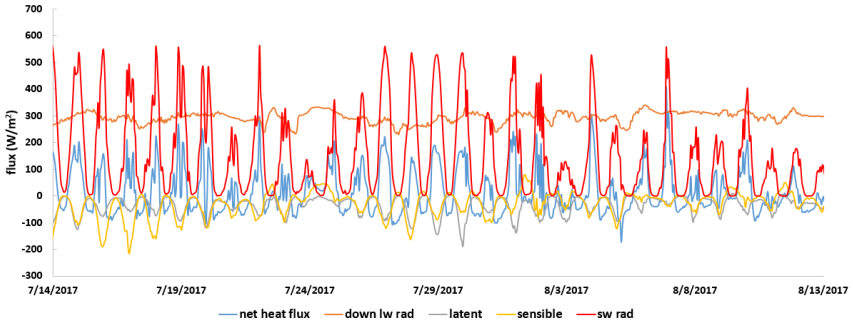

Figure 23. Plot of the 4 of the 5 heat fluxes as well as the net heat flux between July 14 and Aug. 13, 2017 at West Dock, Alaska. Reprinted from Kasper et al., 2023.

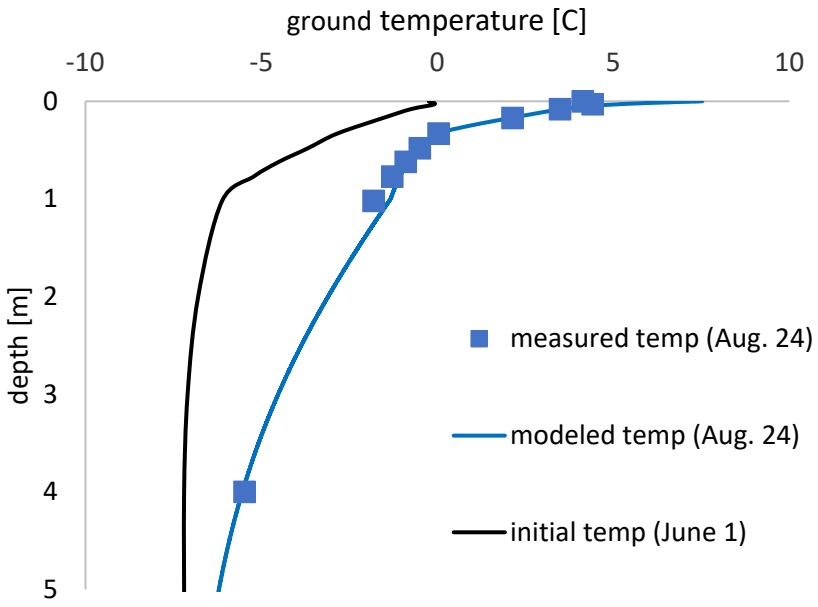

Figure 24. Initial (June 1, 2017) and measured and modelled Aug. 24, 2017 ground temperature, with a flux-type boundary at the tundra surface. Reprinted from Kasper et al., 2023.

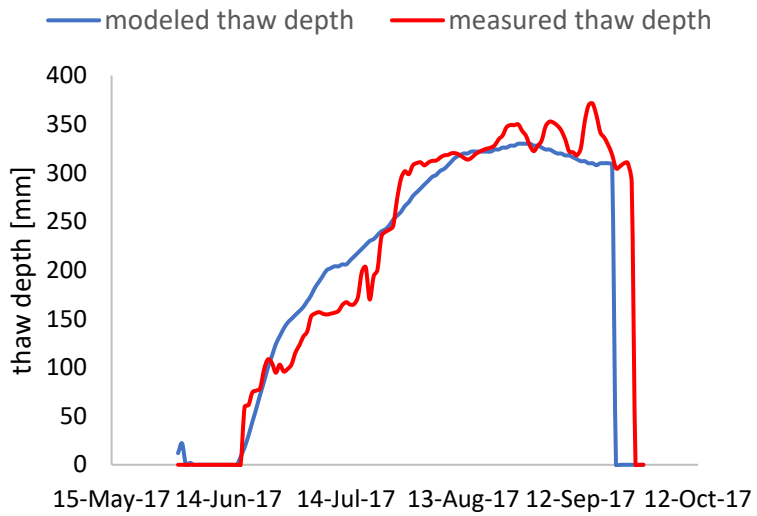

Figure 25. Plot of the measured and modelled thaw depth during the summer of 2017. Reprinted from Kasper et al., 2023.

The *validation* effort described above concerned a vertically oriented temperature profile from the bluff top to a depth of 10 m (Figure 26(a)). We chose the vertical orientation because the available validation data (at West Dock) is along a vertical profile. The *application* of the 1D thermal model in the two-step erosion model, however, requires that the axis of the 1D thermal model be perpendicular to the bluff face as illustrated in the schematic in Figure 26(b). In addition, the 1D thermal model in the two-step model removes any thawed material on the bluff face and daily deposits that material on an equivalent width of beach face, adjacent to the bluff toe.

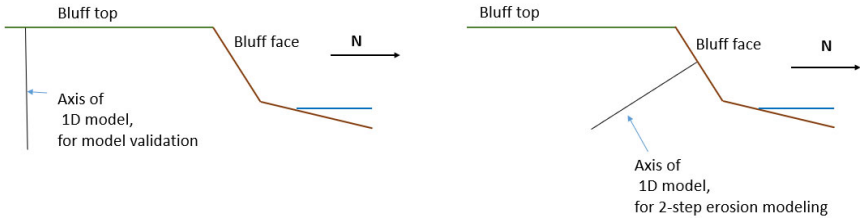

Figure 26. Schematics showing (a) the vertical axis of the 1D thermal model used for model validation and (b) the bluff face-perpendicular axis of the 1D thermal model used for the 2-step erosion modeling. Reprinted from Kasper et al., 2023.

The solar flux calculator

In order to model heat flow along an axis perpendicular to the bluff face, it was necessary to develop a "solar flux calculator" that provided the solar (shortwave) radiation on the typical north-facing coastal bluff, which had a face angle of 45 degrees relative to the horizontal. Although both modelled and measured data on solar radiation on a horizontal surface was available for our study site on the Foggy Island Bay coast, data on north-facing, and angled coastal bluff face was not.

Solar intensity [W/m^2], I, on a flat surface is given by the equation (Buffo, 1972):

$$I = I_0 p^{1/\sin(A)} \sin(\theta) \quad (5)$$

where: I_0 = solar constant: radiation at the top of the atmosphere normal to the sun,
p = atmospheric transmission coefficient (based on altitude, weather),
A = altitude angle off of the horizontal that the sun's rays strike a horizontal surface,
sin (A) = sin (ϕ) sin (δ) +cos(ϕ)cos(δ)cos(h),
ϕ = latitude,
δ = declination (time of year),
h = hour angle,
θ = angle between the surface and the radiation,
Sin (θ)= sin (A)cos($\boldsymbol{\alpha\alpha}$)-cos(A)sin($\boldsymbol{\alpha\alpha}$)sin(Z-$\boldsymbol{\beta\beta}$),
$\boldsymbol{\alpha\alpha}$ = surface slope from horizontal,
Z = azimuth (AZ) CCW from south + 90 degrees,
sin AZ = -cos(δ)sin(h)/cos(A), and
$\boldsymbol{\beta\beta}$ = slope aspect from north (0 is north-facing).

Results – application of the step 1 and step 2 models

The results of the application of the 2-step erosion model for the summer of 2017 are provided in Figure 27. The first inter-storm period extended from June 1, 2017 to July 19 2017. During this time, there were no consequential storm as there were no instances where the water level and wave height simultaneously exceeded 0.4 m. As shown in Figure 23, the solar radiation and the net heat flux are relatively high, so there would have been significant thawing and slumping of the bluff face. Calculations of thaw depth, using the 1D thermal model (step 1 model), find a total thaw depth of 0.51 m during this time period. It is noteworthy that this is significantly above the thaw depth computed and observed with the vertically oriented axis (Figure 25). Since thawed material is removed from the bluff face and placed on the beach face on a daily basis, there is less material on the bluff

face to insulate the deeper layers of the bluff from heat transfer from the atmosphere. The thaw area corresponding to the 0.51 m thaw depth is the product of the depth and the length of the bluff face in the cross-shore direction (about 9.4 m). The deposition of the slumped material is depicted in the beach and bluff profile shown in the upper right of Figure 27.

The first consequential storm of the summer of 2017 occurred on July 20, and it had an offshore surge and wave height of 0.47 m and 6.4 m, respectively. The Xbeach model of this storm computed an erosion area of 1.4 m^2. The eroded portion of the beach face during the July 20 storm is depicted in the profile in lower right of Figure 27. Given that the depth of the active beach was about 7 m, this erosion area corresponds to a linear erosion distance of 0.2 m. Given that the net depositional area from the first inter-storm period was 4.8 m^2, and given that the first storm eroded only 1.4 m^2, we conclude that there was still 3.4 m^2 of material left on the beach face. For simplicity, that material would be assumed to be distributed over the 9.4 wide section of beach face proximal to the bluff toe. The second inter-storm period lasted only 1 day, and it yielded a thaw depth of 0.03 m (corresponding to a depositional area of 0.3 m^2). Hence, following the second inter-storm, the net depositional area was 3.7 m^2 = 3.4 m^2 +.3 m^2 (Figure 24). The two-step model was applied for the remainder of the open water period until freeze-up on Aug. 30, a date determined by temperature observations from the study site.

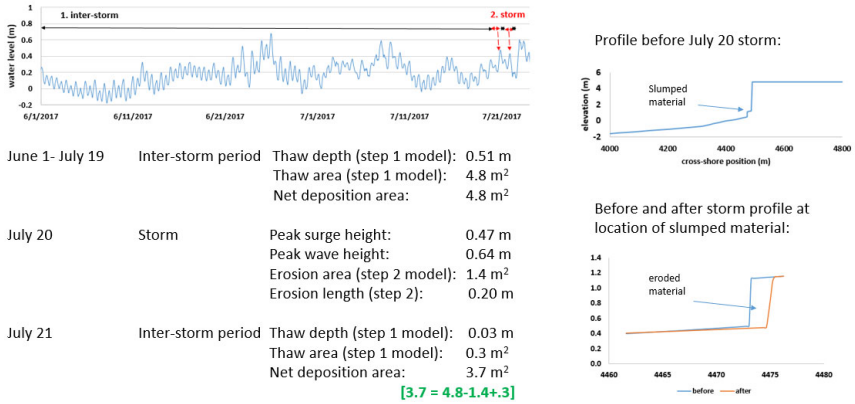

Figure 27. Depiction of details of the two-step erosion model for the summer of 2017. Reprinted from Kasper et al., 2023.

Figure 28 depicts the modelled shoreline erosion between June 1, 2017 and Aug. 30, 2017, based on the two-step model, along with the annual observed erosion

(1.48 m), based on high resolution aerial photos from 2012-2018. The two-step erosion model and erosion measurements are in rough agreement.

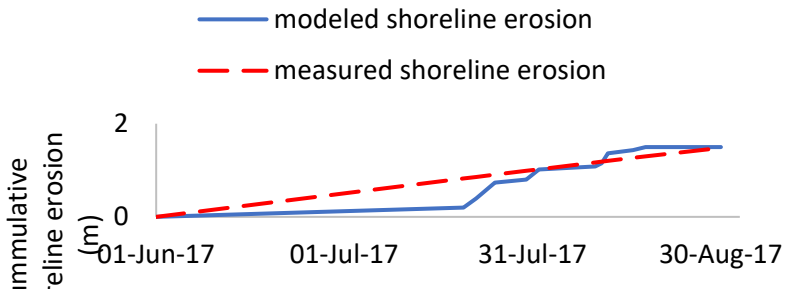

Figure 28. Plot of the modelled and measured shoreline change between June 1, 2017 and Aug. 30, 2017. Reprinted from Kasper et al., 2023.

Discussion of 2-Step Model

In the results section, we reported on the erosion amounts computed by Xbeach. For simplicity, we had used Xbeach to generate a "look-up" table, which provided erosion area as a function of surge height, wave height, and the depth of thawed material on the beach face. Bin sizes for the depth of thawed material were: 0–0.249 m, 0.25–0.499 m, and 0.5–0.749 m. Bin sizes for surge height were: 0.4–0.599 m, 0.6–0.799 m, 0.8–0.999 m, and 1.0–1.199 m. Bin sizes for wave height were: 0.3–0.599 m, 0.6–0.899 m, and 0.9–1.199 m.

We observed no contribution to inter-storm thaw/slump after Aug. 12, 2017 as thawing no longer occurred due to the reduced solar radiation. Ground temperature data indicates that the tundra freezes in late August and we expect no significant storm-induced erosion after this point. We are actively working to compute the freeze-up of the beach face with the Arctic Xbeach model, so we can more definitively address the question of the timing of the freeze-up, and, in particular, how it will change with climate change.

Total offshore transport of material (from the step 2 model) exceeded the amount of bluff face thawed (from the step 1 model) by about 12% in 2017. The fact that these amounts were in rough agreement provided indirect confirmation that the two-step erosion sequence, and the quantitative modeling of the two steps, were reasonable.

The total effective thaw depth into the bluff face in 2017 was computed to be 1.0 m, which greatly exceeded the peak thaw depth on the tundra surface, as expected (Figure 22).

In section 2 of this paper, we discussed how climate change is generally increasing wave heights and periods and, by extending the open water period, it is increasing the number of storm surge events. In section 1, we mentioned that climate change was increasing the temperature of the air and water and accelerating permafrost thaw. In the context of the two-step erosion model developed here, one can readily see that climate change is enhancing both the first and second step – and extending the time period during which the 2-step erosion mechanism can proceed - so we can expect that overall erosion rates due to this mechanism to increase.

Conclusions

In this paper, we have explored Arctic storms and their impacts on coastal geomorphic change. One of the unique aspects of Arctic storms is the importance of the timing of the storms, and, in particular, the state of the sea ice at the time of the storm. With high concentration sea ice present, the wave climate near the coast will be significantly reduced (Rogers, 2019). In this paper, we presented results showing that wave heights near the coast due to Arctic storms have increased dramatically as a consequence of the reduction of sea ice, between 1979 and 2019. Although we did not focus on it here, a second impact of sea ice concentration is storm surge height. The presence of intermediate concentrations of sea ice (e.g. 50% coverage) can increase the wind friction and the surge height (Joyce et al., 2019). The impact of Arctic storms on coastal geomorphic change is also highly dependent on the timing of the storm. A given storm at the beginning of the open water period (e.g., in June), will have a minimal impact compared to its impact later in the open water period when significant thawing of soil and sediment has occurred. Finally, we discussed Arctic storms and their impact on the coast through consideration of the two predominant erosion mechanisms: niche erosion/block collapse and bluff face thaw/slump. We showed how continued climate change and its various impacts is likely to lead to lead to an enhancement of storm-induced erosion regardless of the mechanism.

Acknowledgements

The authors would like to acknowledge contributions from Li Erickson and Anita Engelstad of the USGS and Kees Nederhoff of Deltares USA. We would also like to acknowledge our sources of funding which include (1) Bureau of Ocean Energy Management under Cooperative Agreement M17AC00020, and (2) the National Science Foundation Award #1745508 and #1927789.

References

Barnhart, K.R., Anderson, R.S., Overeem, I., Wobus, C. Clow, G.D. and Urban, F.E. 2014b. Modeling erosion of ice-rich permafrost bluffs along the Alaskan Beaufort Sea coast. J. of Geophysical Research. Earth Science 119:5, 1155-1179. *doi: 10.1002/2013JF002845.*

Buffo, J.M. 1972. Direct solar radiation on various slopes from 0 to 60 degrees north latitude (Vol. 142). Pacific Northwest Forest and Range Experiment Station, Forest Service, US Department of Agriculture.

Garratt, J.R. 1977. Review of drag coefficients over oceans and continents. Monthly Weather Review. 105(7):915-929.

Gibbs, A.E. and Richmond, B.M. 2015. National assessment of shoreline change—Historical shoreline change along the north coast of Alaska, U.S.–Canadian border to Icy Cape: U.S. Geological Survey Open-File Report 2015–1048, 96 p., http://dx.doi.org/10.3133/ofr20151048.

Gibbs, A.E., Richmond, B.M., Palaseanu-Lovejoy, M., Erikson, L.H., Jones, B.M. and Brock, J. 2013. Remote Sensing of the Arctic Coast of Alaska Using Airborne Lidar Data. 2013 American Geophysical Union Fall Meeting. B51H-0406.

Harry, D. G. and Gozdzik, J. S. (1988). Ice wedges: Growth, thaw transformation, and paleo-environmental significance. J. Quaternary Sci., 3: 39–55. doi:10.1002/jqs.3390030107.

Hu, H. Argyropoulos, S.A. 1996. Mathematical modelling of solidification and melting: a review. Modelling and Simulation in Materials Science and Engineering, 4(4):371.

Joyce, B.R., Pringle, W.J., Wirasaet, D., Westerin, J.J., Van der Westhuysen, A.J., Grumbine, R., Feyen, J. 2019. High resolution modeling of western alaskan tides and storm surge under varying sea ice conditions Ocean Modelling. 141(101421):24.

Kasper, J., Erikson, L.H., Ravens, T., Bieniek, P., Englestad, A., Nederhoff, K., Duvoy, P., Fisher, S., Petrone Brown, E. (University of Alaska, Fairbanks and Anchorage, AK and U.S. Geological Survey, Santa Cruz, CA). 2023. Central Beaufort Sea wave and hydrodynamic modeling study. Part I: field measurements and model development. Anchorage (AK): U.S. Department of the Interior, Bureau of Ocean Energy Management, Alaska OCS Region.

XX p. Report No.: OCS Study BOEM 2022-0XX. Contract No.: M17AC00020.

Kobayashi, N. 1985. Formation of Thermoerosional Niches Into Frozen Bluffs Due to Storm Surges on the Beaufort Sea Coast. *J. of Geophysical Research Oceans*, 90(C6): 11983-11988.

Kobayashi, N., Vidrine, J. C., Nairn, R. B. & Soloman, S. M. (1999). Erosion of frozen cliffs due to storm surge on Beaufort Sea Coast. *Journal of coastal research*, 332-344.

Le Roux, J.P. 2009. Characteristics of developing waves as a function of atmospheric conditions, water properties, fetch and duration. Coastal Engineering. 56(4):479–483. https://doi.org/10.1016/j.coastaleng.2008.10.007.

Lüpkes, C., Gryanik, V.M., Hartmann, J., Andreas, E.L. 2012. A parametrization, based on sea ice morphology, of the neutral atmospheric drag coefficients for weather prediction and climate models. Journal of Geophysical Research: Atmospheres. 117(D13).

Lyard, F. H., Allain, D. J., Cancet, M., Carrère, L. and Picot, N.: FES2014 global ocean tide atlas: design and performance, Ocean Sci., 17, 615–649, https://doi.org/10.5194/os-17-615-2021, 2021.

Nederhoff, K., Erikson, L., Engelstad, A., Bieniek, P., Kasper, J. 2022. The effect of changing sea ice on nearshore wave climate trends along Alaska's Central Beaufort Sea coast. The Cryosphere. 16:1609-21629. https://doi.org/10.5194/tc-16-1609-2022.

Overeem, I., Anderson, R. S., Wobus, C. W., Clow, G. D., Urban, F. E. & Matell, N. (2011). Sea ice loss enhances wave action at the Arctic coast. *Geophysical Research Letters*, *38*(17).

Ping, C.-L., Michaelson, G. J., Guo, L., Jorgenson, M. T., Kanevskiy, M., Shur, Y., Dou, F., and Liang, J. 2011. Soil carbon and material fluxes across the eroding Alaska Beaufort Sea coastline, Journal of Geophysical Research. 116, G02004, http://dx.doi.org/10.1029/2010JG001588.

Ravens, T. M. and Peterson, S. 2021. Geologic Controls on Erosion Mechanism on the Alaska Beaufort Coast. *Frontiers in Earth Sciences – Cryospheric Sciences*, 15 October 2021. https://www.frontiersin.org/articles/10.3389/feart.2021.693824/full.

Ravens, T., Ulmgren, M., Wilber, M., Hailu, G., Peng, J. 2017. Arctic-capable geomorphic change modeling with Application to Barter Island, Alaska. IEEE/MTS Oceans Conference. Anchorage Alaska.

Ravens, T. M., Jones B. M., Zhang, J., Arp, C. D. and J. A. Schmutz. 2012. Process-Based Coastal Erosion Modeling for Drew Point, North Slope, Alaska. *J. of Waterway, Port, Coastal, and Ocean Engineering.* 138(2): 122-130.

Ravens, T., Kartezhnikova, M., Ulmgren, M., Yager, G., Jones, B., Erikson, L., Gibbs, A., Richmond, B., Zhang, J., Tweedie, C. and Aguirre, A. 2011. Arctic coastal erosion modeling. Presented at the AGU Fall Meeting, San Francisco, CA, Dec. 2011.

Roelvink, D., Reniers, A. J. H. M., Van Dongeren, A., Van Thiel de Vries, J., Lescinski, J. & McCall, R. (2010). XBeach model description and manual. *UNESCO-IHE Institute for Water Education, Deltares and Delft University of Technology. Report June*, *21*, 2010.

Rogers, W.E., Babanin, A.V., Wang, D.W. 2012. Observation-consistent input and white-capping dissipation in a model for wind-generated surface waves: Description and simple calculations. Journal of Atmospheric and Oceanic Technology, 29(9), 1329–1346. https://doi.org/10.1175/JTECH-D-11-00092.1.

Rogers, W.E. 2019. Implementation of Sea Ice in the Wave Model SWAN. Naval Research Laboratory, Ocean Dynamics and Prediction Branch, Oceanography Division. NRL/MR/7322—19-9874. 32 p.